Turbulence modeling of a single-phase R134a supersonic ejector. Part 1: Numerical benchmark

Sergio Croquer, Sébastien Poncet, Zine Aidoun

Accepted Manuscript

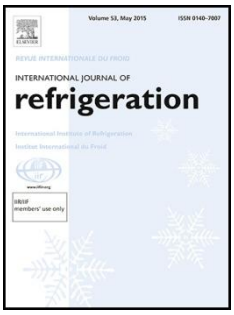

Title: Turbulence modeling of a single-phase R134a supersonic ejector. Part 1: Numerical benchmark

Author: S. Croquer, S. Poncet, Z. Aidoun

PII: S0140-7007(15)00237-6
DOI: http://dx.doi.org/doi:10.1016/j.ijrefrig.2015.07.030
Reference: JIJR 3118

To appear in: *International Journal of Refrigeration*

Please cite this article as: S. Croquer, S. Poncet, Z. Aidoun, Turbulence modeling of a single-phase R134a supersonic ejector. Part 1: Numerical benchmark, *International Journal of Refrigeration* (2015), http://dx.doi.org/doi:10.1016/j.ijrefrig.2015.07.030.

Turbulence modeling of a single-phase R134a supersonic ejector. Part 1: Numerical benchmark

S. Croquer[1]
Université de Sherbrooke, Faculté de génie, Département de génie mécanique 2500 Boulevard de l'Université, Sherbrooke (QC) J1K 2R1, Canada
S. Poncet* [2]
Université de Sherbrooke, Faculté de génie, Département de génie mécanique 2500 Boulevard de l'Université, Sherbrooke (QC) J1K 2R1, Canada
Z. Aidoun[3]
CETC-Varennes, Natural Resources Canada, P.O. Box 4800 1615 Boulevard Lionel Boulet, Varennes (QC), J3X 1S6, Canada

Abstract
The present work reports a numerical analysis of a supersonic ejector in single-phase conditions using R134a as the working fluid. A numerical benchmark of some thermodynamic and two-equation turbulence models have been carried out to highlight the numerical model offering the best compromise between accuracy and calculation cost. The validation is achieved by comparing the predicted entrainment ratio with the experimental data of Garcia del Valle et al. [1]. The $k-\omega$ SST model together with the REFPROP 7.0 database equation appears to be the best combination to predict accurately the ejector performance and capture the shock wave structure. The influence of the outlet temperature, the discussion about the validity of some assumptions made by one-dimensional (1D) models and the exergy analysis within the ejector for the present operating conditions will later be discussed in Part 2 [2].

Highlights
• A supersonic single-phase ejector working with R134a is investigated numerically.
• A numerical benchmark of thermodynamic and turbulence models is performed.
• A real gas equation is necessary to predict accurately the entrainment ratio.
• Oblique shock waves are well captured by the k − ω SST model.

Key words: supersonic ejector, turbulence modeling, R134a refrigerant, shock wave

1 Introduction

The constant increase in energy consumption and decrease in natural resources necessitates a more efficient use of energy. Coupled with the political will to reduce the greenhouse gas emissions, many national initiatives develop to increase the energy efficiency of industrial systems and replace refrigerants with a high environmental impact. In that context, a renewed interest has recently born to incorporate ejectors in refrigeration systems to replace either the expansion valve or the compressor. Besides their lack of moving parts and low maintenance requirements, supersonic ejectors can be driven by renewable or low quality energy sources, such as solar or waste heat sources [3]. Recently, Bilir Sag et al. [4] studied the behavior of a vapor refrigeration cycle with an ejector as the expansion stage. Their exergy analysis of the whole system shows that the ejector expansion refrigeration cycle has a greater overall coefficient of performance by 7 to 12% over the conventional refrigeration cycle. Thus, their application is attractive from an economical, operational and environmental point of view to replace or support conventional compression-expansion devices [5]. Ejectors may be also used to exploit low-

[1] Sergio.Croquer@USherbrooke.ca
[2] * corresponding author, Sebastien.Poncet@USherbrooke.ca - Tel.1 819 821 8000 - 62150
[3] Zine.Aidoun@RNCan-NRCan.gc.ca

pressure reservoirs, industrial vacuum generation, and for gas mixing inside breathing apparatus. The reader can refer to the reviews of Chunnanond and Aphornratana [6], Elbel and Hrnjak [7] and Elbel [8] for a detailed picture of ejector systems in refrigeration or air-conditioning applications.

Numerous experimental or theoretical works have been published over the last decades considering a wide range of refrigerants, various ejector designs and for single and two-phase flows. The literature on supersonic ejectors is then too abundant to draw up an exhaustive state-of-art about the topic. The reader can refer to the review of Milazzo et al. [9] for a recent picture on theoretical and experimental works on ejector refrigeration. In the following, the focus is on single-phase supersonic ejectors.

Given the small dimensions of the ejectors and the need of thermal insulation, experimental studies are frequently limited to global measurements: mass flowrates, temperature and pressure at the inlets and the outlet or more recently wall pressure measurements along the mixing chamber [10]. Attempts have been made by Bartosiewicz et al. [11] to measure the pressure at the centerline of the ejector by invasive pressure probes. Only few works focused on the shock wave structure using local methods. Marinovski et al. [12] investigated the droplet condensation phenomenon occurring in moist air ejector by laser tomography, giving also access to the shock train structure. Bouhanguel et al. [13] extended this work using different illumination sources, polarization directions and types of tracers to investigate specific flow features of a supersonic ejector working with air. Zhu and Jiang [14] studied the shock structure inside two kinds of ejectors by optical Schlieren measurements. They established the shock wave wavelength dependency on the primary inlet to outlet pressure ratio. They showed also that oblique shock waves appear when the ejector reaches the on-design condition, whereas normal shocks appear for off-design operation.

Numerical simulations appear then as a valuable tool to investigate the local flow features inside supersonic ejectors. Due to the relative geometrical complexity of ejectors and most of all to the very complex flow and energy transfer phenomena (shock waves, thin boundary layers, compressibility effects, phase change, etc) involved in the problem, all authors focused on the physics of ejectors by 2D axisymmetric simulations using commercial softwares. Bartosiewicz et al. [11] evaluated the performance of six two-equation turbulence models for single-phase supersonic ejectors. The $k-\varepsilon$ RNG and SST models provided the best overall agreement compared to experimental data. It was partially confirmed by Zhu and Jiang [14], which showed that the $k-\varepsilon$ RNG model agrees better in terms of the shock prediction than the realizable and standard $k-\varepsilon$ and SST models. They suggested a detailed modeling of the near-wall regions to achieve a good prediction of the flow structure inside the ejector. Scott et al. [15, 16] performed extensive calculations using the software Phoenics for a supersonic ejector working woth R245fa. For various geometries and operating conditions, they obtained a very good agreement against experimental data in terms of the entrainment ratio with a maximum deviation of 10.8%. Cai and He [17] studied the effect of different gas and turbulence models and geometry variations on the predictions of a steam supersonic ejector. The ideal gas model underpredicts the entrainment ratio by 20–40%. Recently, Mazzelli and Milazzo [10] performed a combined experimental and numerical analysis of a supersonic ejector chiller with R245fa. Results show that the wall roughness has only a weak effect on the on-design entrainment ratio but can largely reduce the critical back pressure. The global ejector performance depends only slightly on the selected gas model. Pianthong et al. [18] and Sriveerakul et al. [19] were the first to perform 3D numerical simulations for a supersonic steam ejector coming to the same conclusion that there is no

apparent 3D effect. Therefore 2D axisymmetric calculations may be sufficient to investigate such flow configurations. Sriveerakul et al. [19] used a $k-\varepsilon$ realizable turbulence model, the perfect gas equation of state and a coupled-implicit density based solver. Though having obtained a good overall agreement with their own experimental data, the authors suggest the use of real gas models and wall heat transfer. Their work was extended by Ruangtrakoon et al. [20] to quantify the effect of primary nozzle geometries over the local flow features inside the ejector.

All these research groups did not reach a real consensus about the CFD (Computational Fluid Dynamics) model, which could be confidently used to investigate the fluid flow and heat transfer in various types of supersonic single-phase ejectors. Moreover, no particular attention was paid to the influence of the solver or the numerical schemes on the predicted results. The purpose of this work is then to carefully build a CFD model offering the best compromise between accuracy and computational efforts to investigate in details the local flow features of a supersonic single-phase ejector working with R134a. The experimental database established by Garcia del Valle et al. [1] will be used for validation purposes.

The paper is organized as follows: the numerical modeling including the flow parameters, the numerical solver and the thermodynamic and turbulence models are presented in Section 2. Numerical benchmarks of three thermodynamic models and four two-equation turbulence models are performed in Section 3 before some concluding remarks in Section 4. The influence of the outlet temperature on the ejector performance and local flow features and the corresponding exergy analysis among other things will be explained in Part 2 [2].

2 Numerical modeling

Two-dimensional axisymmetric and steady state calculations have been performed using the commercial software ANSYS Fluent v.15 for a single-phase supersonic ejector with R134a as the working fluid. A numerical benchmark of various high- and low-Reynolds number approaches and gas models is achieved considering the ejector recently designed by Garcia et al. [1].

2.1 Geometrical modeling

The geometry and operating conditions are based on the experimental set-up developed by Garcia et al. [1]. They carried out an experimental analysis of three supersonic ejectors (Models A, B and C) with refrigerant R134a. The differences between these three models are both the position of the primary nozzle and the shape of the mixing chamber. Their ejector with the geometry A operates over a wider range of boiler saturation temperatures compared to geometries B and C, while guaranteeing comparable performance. Geometry A has then been considered in this work. Figure 1 shows a schematic view of the geometry, while its main dimensions are summarized in Table 1. The length of the primary nozzle is fixed by the other parameters.

The area ratio A, defined as the ratio between the mixing chamber section and the primary nozzle section, is $A = (D/n_d)^2 = 5.76$ in the present work. According to Huang et al. [21], higher area ratios induce higher values of the entrainment ratio ω with some optimal values around $A = [7-16]$ depending on the flow configurations and refrigerant. The length of the diffuser is here equal to $L = 120.15$ mm $\sqcup 25D$, far from the value $L = 8D$ recommended by Henzler [22]. The present ejector appears to have not been optimally designed. Its other geometrical characteristics are fully displayed in [1].

The geometry of the secondary inlet section is always quite complex in real systems and generally not fully characterized in most of the experimental works. In the experiments of Garcia del Valle et al. [1], the only available information is that the secondary inlet has a classical shape with a 30° half-angle conical entry. Moreover, as the present simulations assume the flow as

being 2D axisymmetric, some assumptions are required to model this part of the ejector. A sensitivity analysis of the secondary inlet geometry has then been carried out to rule out any major influence over the global performance of the ejector. Five different cases have been considered by slightly varying the inclination angles of the secondary inlet walls and the passage section of the secondary fluid. Similar results for the entrainment ratio (maximum deviation of 2.3%) have been obtained for the five distinct geometries (see in [23]). In the following, the geometry A (resp. B) for the secondary inlet, as defined by Croquer et al. [23], has been considered in low- (resp. high-) Reynolds number calculations.

2.2 Flow solver

The governing equations (conservations of mass, momentum and total energy) for a compressible fluid are solved using the commercial software ANSYS Fluent v.15, based on the finite volume method. The flow is assumed as being 2D axisymmetric. To our knowledge, there is indeed no evidence reported in the literature of three-dimensional effects in supersonic ejectors [18]. Unsteady calculations have been first performed but all leading to steady-state solutions. The flow has been then considered in a steady-state regime.

A second-order upwind scheme is used to discretize the advective terms of each equation, except for the pressure equation. For this equation, the PRESTO! scheme designed for flows involving steep pressure gradients has been chosen. The diffusive terms are discretized using second-order central differenced schemes. Gradients are evaluated by a least-square approach.

After the discretization process, a system of algebraic equations is obtained and may be solved using either a density- or pressure-based algorithm. From an historical point of view, a density-based solver is usually required to solve supersonic flows in the presence of shock waves. Recently, pressure-based solvers based on the SIMPLE algorithm or any of its derivatives have nevertheless demonstrated their capability to deal with highly compressible flows with shock waves in single- [14,24] or two-phase [25] flow ejectors. In the present case, the pressure-based algorithm Coupled, with full pressure-velocity coupling has been used for all calculations. The Coupled algorithm solves the momentum and pressure-based continuity equations simultaneously. The full implicit coupling is achieved through an implicit discretization of pressure gradient terms in the momentum equations, and an implicit discretization of the face mass flux, including the Rhie-Chow pressure dissipation terms [26]. The energy equation is solved in a second step and density is computed through an equation of state $\rho = f(P,T)$ (see section 2.3). For this particular application, the Coupled algorithm appeared to be much more stable than any available density-based solvers. A high-order term relaxation technique is also applied throughout the entire computation to ensure convergence smoothness.

2.3 Thermodynamic model

Three different equations of state are considered to evaluate the fluid density ρ of the R134a refrigerant as a function of the thermodynamic variables, pressure P and temperature T:

- the Perfect Gas model. Thermal and hydrodynamic fluid properties are assumed to be constant, apart from the density, which obeys the ideal gas equation. Due to its simplicity, this model is still widely used by different authors to compute supersonic flows in ejectors [11,14,18,19].
- the Redlich-Kwong-Soave (RKS) equation of state. The RKS equation is a pressure explicit cubic three-parameter equation of state (1), known for its simplicity and accuracy [27]. It requires the knowledge of only the critical pressure P_c, critical temperature T_c, acentric factor f and molar mass M of the fluid:

$$P = \frac{R\,T}{v-b} - \frac{a(T)}{v(v+b)} \quad (1)$$

$$a(T) = 0.42748\ \frac{R^2\,T_c^2}{P_c}\,\alpha(T) \quad (2)$$

$$b = 0.08664\ \frac{R\,T_c}{P_c} \quad (3)$$

$$\alpha(T) = \left[1 + (0.480 + 1.574\,f - 0.176\,f^2)\left(1 - \left(\frac{T}{T_c}\right)^{1/2}\right)\right]^2 \quad (4)$$

- the REFPROP 7.0 equation database. The REFPROP model [28] for refrigerant R134a is based on the formulation of Tillner-Roth and Baehr [29]. Fluid thermodynamic and transport properties (viscosity, specific heat, and thermal conductivity) are computed using the Helmholtz free energy equation of state. This equation depends on 21 parameters, obtained from statistical analysis and least-square fitting of the most accurate R134a measurements available at that time [29]. This model accurately represents real gas behavior in the temperature range [170–455] K and for pressures up to 70 MPa.

For the perfect gas model, all thermo-physical properties (viscosity, specific heat, and thermal conductivity) are considered as constant and fixed to the average between the inlet and outlet values. The same procedure has been applied for the RKS model in terms of viscosity and thermal conductivity. **The specific heat capacity is related to differentials of pressure according to temperature and density through the RKS equation of state.** For all models and whatever the operating conditions (see Table 2), the fluid is assumed to remain in the gas phase. Its properties are summed up in Table 3.

2.4 Turbulence modeling

Various two-equation turbulence models available within Fluent v.15 have been compared to the experimental data of Garcia del Valle et al. [1] in their high- or low-Reynolds number formulation. In their high-Reynolds number form, the following four two-equation turbulence models have been considered:

- a standard $k-\varepsilon$ model, known for its robustness, economy, and reasonable accuracy over a wide range of turbulent flows. The assumption is that the flow is fully turbulent and the effects of viscosity are negligible;
- a $k-\varepsilon$ RNG model. This model is derived from the instantaneous Navier-Stokes equations, using a "renormalization group" (RNG) method. The analytical derivation results in a model with constants different from those in the standard $k-\varepsilon$ model, and additional terms and functions in the transport equations for the turbulence kinetic energy k and its dissipation rate ε;
- a $k-\varepsilon$ Realizable model. This model is an improved version of the first two ones. The turbulence viscosity is evaluated in a different way and a new transport equation for the dissipation rate ε has been derived from an exact equation for the transport of the mean-square vorticity fluctuation taking into account some mathematical constraints. It is expected that this model is able to predict a more accurate spreading rate of the jet [26] at the outlet of the primary nozzle.
- a shear-stress transport (SST) $k-\omega$ model. The SST model is an hybrid model, which blends the accurate formulation of the standard $k-\omega$ model in the near-wall region with the free-stream independence of the $k-\varepsilon$ model in the far field. Compared to the standard $k-\omega$ model, it

incorporates also a damped cross-diffusion derivative term in the transport equation of the specific dissipation rate ω and the turbulence viscosity is modified to account for the transport of the turbulent shear stress.

The flow in the near-wall regions is not directly computed by such approaches but rather approximated using appropriate wall functions, which relax the constraints in terms of required mesh grids in these regions and then considerably reduces the computational time. All these two-equation models in their high-Reynolds number formulation offer a relatively good compromise between accuracy and computational cost even if none of them is capable of having good performance for all possible flow configurations. It appears then necessary to perform a numerical benchmark of these models for the specific ejector system designed by Garcia del Valle et al. [1].

For the low-Reynolds number approach, only the $k-\omega$ SST model has been considered in the following. The reasons are twofold: some previous numerical studies [11,14] showed its overall superiority over low-Reynolds number $k-\varepsilon$ models and computations using the standard $k-\varepsilon$ model in its low-Reynolds number formulation were found here to be more unstable for this range of operating conditions.

2.5 Numerical settings

Three operating conditions corresponding to the experiments of Garcia del Valle et al. [1] have been considered in the present work. At both inlets and the outlet, the pressure is prescribed based on the saturation temperature, denoted T_{sat}. The compression ratio P^{ratio}, defined as the ratio of static pressures between the outlet and the secondary inlet, is then an input in the present simulations. All values for the saturation temperatures and static pressures imposed at the inlets and the outlet are displayed in Table 2 together with the experimental values of the entrainment ratio ω_{exp} and the computed compression ratio P^{ratio}. It is noticeable that inlet temperatures include an overheat of $10\ ^{o}C$ (e.g. the primary fluid temperature for OP 1 is fixed to $89.37\ ^{o}C$ at the inlet). These working conditions are particularly appropriate and suitable for refrigeration systems. The low boiler temperatures enable heat utilization from various cheap sources such as industrial waste heat or renewable energy sources, at the same time the low evaporator temperatures enable to meet the refrigerating or air-conditioning requirement (heat is rejected by the compression cycle) while guaranteeing a good performance of the system. It guarantees also the absence of condensation phenomena, allowing for the adoption of a more simpler gas model. One recalls that the flow is assumed to be steady-state and 2D axisymmetric, neglecting three-dimensional effects [18]. Compared to the average velocities reached inside the ejector, velocities at the inlets and the outlet are almost negligible. Thus, the total values for pressure and temperature are supposed to be equal to their static values, which is a usual approximation in CFD analysis of supersonic ejectors. Turbulence intensities at the inlets are set at 5%. It has been checked that considering other turbulence levels lead to indistinguishable results.

Walls are considered as adiabatic and hydrodynamically smooth surfaces. Mazzelli and Milazzo [10] showed that imposing an arithmetic roughness height equal to 3.5 μm improved the numerical results by slightly decreasing the entrainment ratio. Some numerical tests have been done here for two values of the roughness height: $2\mu m$ and $20\mu m$, keeping in mind that such quantity is not available in the experiments of Garcia del Valle et al. [1]. Even for the lowest value, the predicted entrainment ratio drops far below the experimental values for OP2 and OP3 exhibiting all features of off-design conditions. For example, for OP3, the numerical predictions **using the standard $k-\varepsilon$ model and the REFPROP database** give ω = 0.232 for a roughness

height equal to 2μm and 0.028 for 20μm, which is to be compared to the experimental value $\omega_{exp} = 0.339$. All turbulence models provide similar results and confirm the results of Mazzelli and Milazzo [10], who reported the same steepness and extension of the off-design region for similar condenser temperatures. The inner surface of the ejector designed by Garcia del Valle et al. [1] may be considered as a mirror-like surface and as a smooth wall in the CFD model.
An hybrid initialization based on boundary interpolation methods is used to start the calculations. A Laplace equation is solved to determine the velocity and pressure fields from the imposed boundary conditions. All other variables, such as temperature or turbulence quantities, are automatically patched based on domain averaged values.
A mesh sensitivity analysis was carried out for both low- and high-Reynolds number approaches to ensure the independence of the solution from the spatial discretization:

- For all turbulence models based on a high-Reynolds number formulation, the mesh grid was built using *ANSYS Meshing software v.15* with standard wall functions for the near-wall treatment. An unstructured type mesh is used with 5 prismatic layers in the near-wall regions. A mesh grid with 51000 cells has proven to be sufficient to get grid independent solutions [23]. The maximum value for the wall coordinate remains then in the range [20–30] depending on the RANS model, which is usually required when using wall functions.
- For the low-Reynolds number approach, the software *ANSYS ICEM v.15* was used to build the structured mesh grid. It is composed of tetrahedral elements, which allows a greater control over the near-wall elements and their growing rate towards the free flow area. A mesh grid with 645000 elements proves to be sufficient to get grid independent solutions. The wall coordinate remains less than 0.79, which ensures to have at least 18 mesh points to describe the linear and logarithmic regions of the velocity profile [30].

Details of the chosen grids are shown in Figure 2. In all cases, a mesh refinement in the radial direction is necessary in the mixing layer appearing at the trailing edge of the primary nozzle. As the mesh grids are sufficiently refined in the streamwise direction for both approaches, the adaptative mesh option does not improve the predictions of the CFD model and has been then switched off to reduce the calculation time.
Convergence is achieved when stable values of the static outlet temperature, total mass flow across the domain and residuals are under 10^{-4} for all conservation equations. It is typically reached shortly after 1000 iterations. All the computations have been performed using a workstation with 16 GB of RAM and a 4 core 3.40 GHz CPU. In average, the calculation time is around 1 hour and 3 hours for the high- and low-Reynolds number approaches respectively using 3 processors.

3 Results and discussion

The results are compared to the experimental database of Garcia del Valle et al. [1] and discussed in terms of the entrainment ratio and the shock wave structure for three thermodynamic and four turbulence models.

3.1 Influence of the thermodynamic model

The present ejector uses the 1,1,1,2-tetrafluoroethane ($C_2H_2F_4$), also known as R134a or HFC-134a refrigerant. It is an environmentally benign fluid classified in the AHSRAE safety group A1 (not toxic and nonflammable). For these reasons, it has been gradually replacing more hazardous refrigerants like the HCFC22 in refrigeration or road transport systems. Its boiling point is $-26.3°C$ such that R134a is always in gas phase for the present application. An equation of state is then required to evaluate its density $\rho(P,T)$, which strongly depends on local pressure P and

temperature T. The calculations have been performed using the standard $k-\varepsilon$ model in its high-Reynolds number formulation for three equations of state.

Figure 3 compares the three gas models in terms of the entrainment ratio ω for the three operating points. The perfect gas model fails to predict the good entrainment ratio whatever the operating conditions. The maximum deviation compared to the experimental values of Garcia del Valle et al. [1] is up to 19% at OP2 and OP3. The two real gas models provide essentially the same results with a very good agreement for OP1, the deviation with the experimental value being less than 1%. At OP 2 (resp. OP 3), deviations are 4.4% (resp. 5.8%) and 6% (resp. 3.4%) for the REFPROP 7.0 and RKS models respectively. The slightly overprediction of the entrainment ratio ω increases for increasing values of the outlet pressure but the two real gas models show negligible differences among each other, such that no definitive conclusion can be drawn. **Even if different ejectors, operating conditions and refrigerants have been considered, the present results do not support the conclusions of Garcia del Valle et al. [31]. The authors showed indeed using an innovative 1D model based on a potential flow approach that real or ideal gas behaviors lead to very similar results in terms of entrainment ratio. It supports the conclusion that no universal 1D or CFD model may be recommended.**

To go into more details, Figures 4a and b display the distributions of the static pressure and Mach number respectively in the streamwise direction at the centerline of the ejector for OP2. All three models provide essentially the same profiles with a normal shock wave of relatively weak intensity located around $x = 0.04$ m at the outlet of the mixing chamber. As can be seen from the two zooms, the exact position of the shock wave slightly depends on the thermodynamic model. Garcia del Valle et al. [1] suggested that a system of shock waves appeared in the mixing area and it will be shown in Section 3.2 that this discrepancy is more related to the choice of the turbulence model.

Table 3 summarizes the main thermo-physical properties used or calculated by the three thermodynamic models. It shows in particular the importance of using real gas models **as the heat capacity (and so the Prandtl number) may** vary in a large range. Surprisingly, both real gas models predict very different results for the Prandtl number and the heat capacity, while predicting the same entrainment ratio and Mach and pressure distributions.

It may be of interest also to look at the distribution of the compressibility factor Z in this case. The compressibility factor is the ratio of the molar volume of a gas to the molar volume of an ideal gas at the same temperature and pressure and is evaluated through the equation of state. It may be seen as a useful indicator of the deviation from the perfect gas model. Figure 5 displays the map of Z obtained by the model based on the REFPROP 7.0 database equation for OP2. The factor Z varies from 0.648 at the inlet of the primary nozzle to 0.935 in the constant section area where the shock wave appears. As expected, the deviation from the perfect gas law is then maximum at the inlet of the primary nozzle where the highest pressure levels are reached. Z is equal to 0.91 in the secondary fluid entrance region, close to the behavior of a perfect gas. The overprediction already evoked above in terms of the entrainment ratio is then related to inaccurate predictions of the heat and fluid flow inside the primary nozzle. Similar results have been obtained using the RKS equation of state with $0.672 \leq Z \leq 0.967$.

As a conclusion, the use of the perfect gas model to investigate supersonic ejectors working with R134a, though being more easy to use, is not advisable. The two real gas models perform quite well providing very similar results in terms of ejector performance and local flow features. It has been checked also that there is no noticeable difference between the two real gas models in terms

of computational resources (CPU time and required memory size). Thus, they can be used confidently for supersonic ejector applications with R134a. For sake of clarity, only the REFPROP 7.0 database equation will be considered in the following. For other ejector designs and other operating conditions, this model should nevertheless be used with a certain caution as the temperature range covered by this database (170–455K) could be easily exceeded during the convergence process, which would cause the solution to fall in regions where the fluid properties are not defined. It may be particularly true during the first statistical iterations where the calculations are highly oscillating if initial conditions are not carefully chosen. Using the REFPROP 7.0 database, Mazzelli and Milazzo [10] obtained a very low convergence rate of the solution and a weak stability for a supersonic ejector working with R245fa recommending the use of the Peng-Robinson model.

3.2 Influence of the RANS turbulence model

Four two-equation turbulence models described in Section 2.4 have been compared to the experimental data of Garcia del Valle et al. [1]. For all calculations, the real gas model based on the REFPROP 7.0 database has been used.

Table 4 shows the relative deviation $\varepsilon = |\omega_{pred} - \omega_{exp}| / \omega_{exp}$ between the predicted ω_{pred} and the experimental $\omega_{exp} = 0.398$ values of the entrainment ratio for OP2. The standard $k-\varepsilon$ model with standard wall functions performs the best with a deviation of 4.27%. This model is indeed known to predict well wall-bounded flows with relatively smooth mean pressure gradients, which is the case in the region confined between the primary nozzle exit and the appearance of the shock wave in the mixing chamber. The advanced versions of the $k-\varepsilon$ model (realizable $k-\varepsilon$ and $k-\varepsilon$ RNG) do not improve the predictions of the entrainment ratio. By comparing the low- and high-Reynolds number $k-\omega$ SST models, it is shown that modeling the flow up to the walls slightly improves the predictions of the entrainment ratio. The present results confirm those obtained by Hemidi et al. [32], who showed that the standard $k-\varepsilon$ model in its high-Reynolds number formulation performs better than the high-Reynolds number $k-\omega$ SST model.

Figure 6 compares the numerically predicted operation curves obtained by three turbulence models to the experimental data reported by Garcia et al. [1]. There is a good overall agreement between the standard $k-\varepsilon$, the $k-\omega$ SST in its low-Reynolds number approach and the experimental results. The difference is around 4% along the on-design conditions ($T_{sat} < 33°$). According to these models, the critical operation point is $T_{sat} = 33°$, which marginally differs from the experimental value $T_{sat} = 32.5°$. Off-design conditions operate up to approximately $T_{sat} = 36°$, which corresponds to the breakdown pressure and to the beginning of the ejector malfunction region. As a conclusion, the low-Reynolds number approach significantly improves the predictions of the entrainment ratio for a given $k-\omega$ SST model, reproducing well the ejector global performance. **In other ejector designs and for other operating conditions, Hemidi et al. [32] reported a deviation of** 10% **for a supersonic air ejector and Sriveerakul et al. [19] obtained deviations up to** 12.9%**.**

Both the standard $k-\varepsilon$ and low-Reynolds number $k-\omega$ SST models predict quite well the same entrainment ratio over the whole operation curve. Nevertheless, as shown by Hemidi et al. [33], the local flow features and especially the shock wave structure may differ significantly. Figure 7 displays the static pressure profile and Mach number distribution along the centerline of the ejector for OP2. Both graphs clearly show that a normal shock wave appears in the mixing chamber, around x = 0.035 m for the standard $k-\varepsilon$ model. The other $k-\varepsilon$ models predict the

same normal shock wave but for a position slightly downstream, around x = 0.03 m for the $k-\varepsilon$ RNG model and x = 0.0325 m for the realizable $k-\varepsilon$ model. On the other hand, the $k-\omega$ SST predicts a series of oblique shock waves further downstream in this region, around x = 0.024 m. Information about the nature of the shock wave is relatively limited in the literature. Though having considered different ejector geometries and refrigerants, the experimental flow visualizations of Bouhanguel et al. [13], the density field observations of Zhu and Jiang [14] or the numerical simulations of Bartosiewicz et al. [34] and Scott et al. [16] all report a train of oblique shock waves. The low-Reynolds number $k-\omega$ SST model predicts a shock train with a relatively lower intensity as the amplitude of the pressure and Mach number oscillations are smaller than those predicted by the high-Reynolds number approach.

Figure 8 displays the iso-contours of the Mach number in the mixing region at the critical conditions for three turbulence models. It confirms that the standard $k-\varepsilon$ model predicts a single normal shock wave occurring towards the end of the mixing chamber. On the other hand, the low- and high-Reynolds number $k-\omega$ SST models predict the existence of a shock train in the second half of the mixing chamber. Nevertheless, the high-Reynolds number $k-\omega$ SST model slightly anticipates the formation of the shock train. It is interesting to note that the good capture of the shock train structure is inherent to the turbulence model as both $k-\omega$ SST with high- or low-Reynolds number formulations provide the same results, while very different mesh grid arrangements are used. It is not so surprising as the $k-\omega$ SST uses a $k-\omega$ formulation in the inner parts of the boundary layer, which makes the model directly usable all the way down to the wall through the viscous sublayer. It has been designed as a low-Reynolds number turbulence model without any extra damping functions even its high-Reynolds number formulation. The SST formulation also switches to a $k-\varepsilon$ behaviour in the free-stream and thereby avoids the common $k-\varepsilon$ problem that the model is too sensitive to the inlet free-stream turbulence properties. The $k-\omega$ SST low-Reynolds number combines then the good prediction of the shock-structure by the high-Reynolds number $k-\omega$ SST model and of the entrainment ratio by the high-Reynolds number $k-\varepsilon$ model.

To go a little further and try to explain the different behaviors between these two-equation models, Figure 9 shows the contours of the turbulence kinetic energy k (m^2/s^2) obtained by the standard $k-\varepsilon$ and $k-\omega$ SST models in their high-Reynolds number formulation for OP2. The maps obtained by the other models exhibit quite comparable results and are then not shown here. Turbulence kinetic energy reaches particularly high values in two regions within the ejector: the **shear-**layer, which develops at the trailing edge of the primary nozzle exit and at the exact location of the shock wave in the **constant section area**. Within the **shear-**layer, the maximum values of k are equal to 1475 and 1780 m^2/s^2 for the standard $k-\varepsilon$ and $k-\omega$ SST models respectively. This maximum value gets 1690 and 2440 m^2/s^2 for the RNG and realizable models respectively. The high values of the turbulence kinetic energy in the **shear-**layer are directly connected to the high values of the entrainment **ratio**. At the shock wave location, the standard $k-\varepsilon$ and $k-\omega$ SST models predict very different values for the maximum of the turbulence kinetic energy k_{max} : k_{max} = 3170 m^2/s^2 for the standard $k-\varepsilon$ model and k_{max} □ 10^3 m^2/s^2 for the $k-\omega$ SST model.

Another interesting quantity when speaking about turbulence modeling is the turbulence viscosity ratio defined as the ratio of the turbulence viscosity ν_T and the kinematic viscosity ν. As shown in Table 3, the viscosity ν varies within the ejector when using the REFPROP 7.0 database. It has been checked that the same contours are obtained for ν whatever the two-equation model used. The turbulence viscosity ratio is then a direct measure of the turbulence viscosity ν_T and so

of the energy dissipated by the turbulence model. Figures 10a and b report the iso-contours of the turbulence viscosity ratio for OP2 using the standard $k-\varepsilon$ and $k-\omega$ SST high-Reynolds number models. Both models exhibit the same patterns. The turbulence models act mainly in the mixing layer at the trailing edge of the primary nozzle exit and then at the shock wave location. The maximum turbulence viscosity ratio is observed in all cases downstream of the shock waves at the end of the mixing chamber or at the inlet of the diffuser. It is noteworthy that the standard $k-\varepsilon$ model is much more dissipative and especially at the shock wave location.

It is noticeable that the maps of the turbulence kinetic energy and the turbulence viscosity ratio are the same between the two $k-\omega$ SST models with slightly different maximum values. For the low-Reynolds approach, $k_{max} = 1793 \quad m^2/s^2$ and $(\nu_T/\nu)_{max} = 16614$. The structure and the position of the shock wave seem to be better captured by the $k-\omega$ SST model either in its high- or low-Reynolds number formulation. The low-Reynolds approach improves the predictions of the flow field within the boundary layers. The secondary fluid passage being confined close to the wall of the mixing chamber, the value of the predicted entrainment ratio is also improved. On the other hand, the advanced versions of the $k-\varepsilon$ model do not improve the predictions of the standard model both in terms of the global performance and the more local flow features within the ejector.

4 Conclusion

The flow structure and performance characteristics of a supersonic ejector working with R134a have been studied by 2D axisymmetric, steady-state numerical simulations and compared to the experimental data of Garcia del Valle et al. [1]. A numerical benchmark of some thermodynamic and two-equation turbulence models available within Fluent v.15 have been performed to build the CFD model offering the best compromise between accuracy and computational efforts. The following main conclusions may be drawn:

- The two real gas equations, the Redlich-Kwong-Soave equation of state and the REFPROP 7.0 database equation, provide similar and good results, while the perfect gas law fails to predict the correct entrainment ratio with an overprediction of about 20% whatever the operating conditions.
- The standard $k-\varepsilon$ in its high-Reynolds number formulation provides the best agreement in terms of entrainment ratio with a deviation of less than 1% from the experimental value for OP1. This deviation slightly increases when the outlet pressure increases. On the other hand, it predicts a normal shock wave in the mixing chamber instead of an oblique shock train, which is better captured by the $k-\omega$ SST model either in its high- or low-Reynolds number formulation. The maximal deviation for these three models is 4% in terms of entrainment ratio for the three operating conditions.
- Though requiring a calculation time three times longer, the $k-\omega$ SST model in its low-Reynolds number formulation offers the best overall agreement, being capable of capturing the detailed structure of the shock train. As 3D calculations are not required, it appears as a very promising tool even from an engineering point of view to design future ejectors as converged states are achieved within 3 hours with standard computational resources.

The CFD model based on the $k-\omega$ SST model in its low-Reynolds number formulation and the REFPROP 7.0 database equation can be now used confidently to investigate, in the second part of this work, the local flow features and the exergy destruction within the ejector and discuss the different assumptions made by 1D thermodynamic models.

Acknowledgement

This project is part of the research program of the NSERC Chair in Industrial Energy Efficiency, established at Université de Sherbrooke in 2014, with the support of Hydro-Québec, Canmet-

Énergie, Rio Tinto Alcan and the Natural Sciences and Engineering Research Council of Canada. They are here gratefully acknowledged. The authors acknowledge also Professor Nicolas Galanis for fruitful discussions and critically reviewing the manuscript.

References

[1] J. García del Valle, J.M. Saíz Jabardo, F. Castro Ruiz, and J.F. San José Alonso. An experimental investigation of a R134a ejector refrigeration system. *International Journal of Refrigeration*, 46:105–113, 2014.

[2] S. Croquer, S. Poncet, and Z. Aidoun. Turbulence modeling of a single-phase R134a supersonic ejector. Part 2: Local flow structure and exergy analysis. *International Journal of Refrigeration*, submitted, 2015.

[3] A.J. Meyer, T.M. Harms, and R.T. Dobson. Steam jet ejector cooling powered by waste or solar heat. *Renewable Energy*, 34:297–306, 2009.

[4] N. Bilir Sag, H.K. Ersoy, A. Hepbasli, and H.S. Halkaci. Energetic and exergetic comparison of basic and ejector expander refrigeration systems operating under the same external conditions and cooling capacities. *Energy Conversion and Management*, 90:184–194, 2015.

[5] K. Sumeru, H. Nasution, and F.N. Ani. A review on two-phase ejector as an expansion device in vapor compression refrigeration cycle. *Renewable and Sustainable Energy Reviews*, 16(7):4927–4937, 2012.

[6] K. Chunnanond and S. Aphornratana. Ejectors: applications in refrigeration technology. *Renewable and Sustainable Energy Reviews*, 8(2):129–155, 2004.

[7] S. Elbel and P. Hrnjak. Ejector refrigeration: an overview of historical and present developments with an emphasis on air-conditioning applications. In *Int. Refrigeration and Air Conditioning Conference*, pages 2350–1–2350–8, Purdue, 2008.

[8] S. Elbel. Historical and present developments of ejector refrigeration systems with emphasis on transcritical carbon dioxide air-conditioning applications. *International Journal of Refrigeration*, 34:1545–1561, 2011.

[9] A. Milazzo, A. Rocchetti, and I.W. Eames. Theoretical and Experimental Activity on Ejector Refrigeration. *Energy Procedia*, 45:1245–1254, 2014.

[10] F. Mazzelli and A. Milazzo. Performance analysis of a supersonic ejector cycle working with R245fa. *International Journal of Refrigeration*, 49(0):79–92, 2015.

[11] Y. Bartosiewicz, Z. Aidoun, P. Desevaux, and Y. Mercadier. Numerical and experimental investigations on supersonic ejectors. *International Journal of Heat and Fluid Flow*, 26(1):56–70, 2005.

[12] T. Marinovski, P. Desevaux, and Y. Mercadier. Experimental and numerical visualizations of condensation process in a supersonic ejector. *Journal of Visualization*, 12(3):251–258, 2009.

[13] A. Bouhanguel, P. Desevaux, and E. Gavignet. Flow visualization in supersonic ejectors using laser tomography techniques. *International Journal of Refrigeration*, 34:1633–1640, 2011.

[14] Y. Zhu and P. Jiang. Experimental and numerical investigation of the effect of shock wave characteristics on the ejector performance. *International Journal of Refrigeration*, 40:31–42, 2014.

[15] D. Scott, Z. Aidoun, O. Bellache, and M. Ouzzane. CFD simulations of a supersonic ejector for use in refrigeration applications. In *International Refrigeration and Air Conditioning Conference*, pages 2159–1–2159–8, Purdue, 2008. Purdue.

[16] D. Scott, Z. Aidoun, and M. Ouzzane. An experimental investigation of an ejector for validating numerical simulations. *International Journal of Refrigeration*, 34:1717–1723, 2011.

[17] L. Cai and M. He. A Numerical Study on the Supersonic Steam Ejector Use in Steam Turbine System. *Mathematical Problems in Engineering*, 2013:1–9, 2013.
[18] K. Pianthong, W. Seehanam, M. Behnia, T. Sriveerakul, and S. Aphornratana. Investigation and improvement of ejector refrigeration system using computational fluid dynamics technique. *Energy Conversion and Management*, 48(9):2556–2564, 2007.
[19] T. Sriveerakul, S. Aphornratana, and K. Chunnanond. Performance prediction of steam ejector using computational fluid dynamics: Part 1. Validation of the CFD results. *International Journal of Thermal Sciences*, 46(8):812–822, 2007.
[20] N. Ruangtrakoon, T. Thongtip, S. Aphornratana, and T. Sriveerakul. CFD simulation on the effect of primary nozzle geometries for a steam ejector in refrigeration cycle. *International Journal of Thermal Sciences*, 63:133–145, 2013.
[21] B.J. Huang, J.M. Chang, C.P. Wang, and V.A. Petrenko. A 1-D analysis of ejector performance. *International Journal of Refrigeration*, 22:354–364, 1999.
[22] H.J. Henzler. Design of ejectors for single-phase material systems. *German Chemical Engineering*, 6:292–300, 1983.
[23] S. Croquer, S. Poncet, and Z. Aidoun. Étude numérique d'un éjecteur monophasique fonctionnant au R134a. In *12e Colloque Interuniversitaire Franco-Québécois sur la Thermique des Systèmes*, pages 1–6, Sherbrooke, 2015.
[24] M. Yadzani, A.A. Alahyari, and T.D. Radcliff. Numerical modeling of two-phase supersonic ejectors for work-recovery applications. *International Journal of Heat and Mass Transfer*, 55:5744–5753, 2012.
[25] C. Li and Y.Z. Li. Investigation of entrainment behavior and characteristics of gas-liquid ejectors based on CFD simulation. *Chemical Engineering Science*, 66:405–416, 2011.
[26] *ANSYS FLUENT Theory Guide release 15.0, ANSYS Inc.*, 2013.
[27] R. Camporese, G. Bigolaro, and L. Rebellato. Calculation of thermodynamic properties of refrigerants by the Redlich-Kwong-Soave equation of state. *International Journal of Refrigeration*, 8(3):147–151, 1985.
[28] *NIST Reference Fluid Thermodynamic and Transport Properties - REFPROP, v9.0*, 2010.
[29] R. Tillner-Roth and H.D. Baehr. An International Standard Formulation for the Thermodynamic Properties of 1,1,1,2-tetrafluoroethane (HFC-134a) for Temperatures From 170K to 455K and Pressures up to 70MPa. *Journal of Physical and Chemical Reference Data*, 23(5):657–729, 1994.
[30] S. Croquer, S. Poncet, and Z. Aidoun. Operation and exergetic analysis of a supersonic R134a ejector by low-Reynolds number turbulence model. In *24th International Congress of Refrigeration*, pages 1–8, Yokohama, 2015.
[31] J. García del Valle, J.M. Sáiz Jabardo, F. Castro Ruiz, and J. San José Alonso. A one-dimensional model for the determination of an ejector entrainment ratio. *International Journal of Refrigeration*, 35(4):772–784, 2012.
[32] A. Hemidi, F. Henry, S. Leclaire, J.-M. Seynhaeve, and Y. Bartosiewicz. CFD analysis of a supersonic air ejector. Part I: Experimental validation of single-phase and two-phase operation. *Applied Thermal Engineering*, 29(8–9):1523–1531, 2009.
[33] A. Hemidi, F. Henry, S. Leclaire, J.-M. Seynhaeve, and Y. Bartosiewicz. CFD analysis of a supersonic air ejector. Part II: Relation between global operation and local flow features. *Applied Thermal Engineering*, 29(8-9):2990–2998, 2009.

[34] Y. Bartosiewicz, Z. Aidoun, and Y. Mercadier. Numerical assessment of ejector operation for refrigeration applications based on CFD. *Applied Thermal Engineering*, 26(5–6):604–612, 2006.

Figure 1. Schematic view of the ejector with relevant notations.

Figure 2. Details of the mesh grids used for the high- and low-Reynolds number turbulence models.

Figure 3. Entrainment ratio ω for the three operating points. Comparisons between three gas models using the standard $k-\varepsilon$ model and the experimental data of Garcia del Valle et al. [1].

Figure 4. Comparisons of the gas models for OP2: (a) static pressure profile P (kPa) and (b) Mach number Ma distribution along the centerline of the ejector. Results obtained using the standard $k-\varepsilon$ model.

Figure 5. Map of the compressibility ratio Z obtained by the standard $k-\varepsilon$ model with the REFPROP 7.0 database for OP2.

Figure 6. Ejector operation curve for a saturation temperature at the primary inlet equal to $T_{sat} = 84.39°C$. Comparisons between three turbulence models and the experimental data of Garcia del Valle et al. [1]. Results obtained using the REFPROP 7.0 database equation.

Figure 7. Comparisons of the turbulence models for OP2: (a) static pressure profile P (kPa) and (b) Mach number Ma distribution along the centerline of the ejector. Results obtained using the REFPROP 7.0 database equation. HRN (resp. LRN) refers to a high- (resp. low-) Reynolds number approach.

Figure 8. Iso-contours of the Mach number in the mixing region for OP2. Comparisons between the standard $k-\varepsilon$ and the high- and low-Reynolds number $k-\omega$ SST models.

Figure 9. Maps of the turbulence kinetic energy k (m^2/s^2) for OP2: (a) standard $k-\varepsilon$ and (b) $k-\omega$ SST in their high-Reynolds number formulation. Results obtained using the REFPROP 7.0 database equation.

Figure 10. Maps of the turbulence viscosity ratio ν_T/ν for OP2: (a) standard $k-\varepsilon$ and (b) $k-\omega$ SST in their high-Reynolds number formulation. Results obtained using the REFPROP 7.0 database equation.

Table 1
Main dimensions of the ejector.

Parameter	**Value** [*mm*]
Primary nozzle throat diameter, n_d	2.00
Primary nozzle exit diameter, d	3.00
Nozzle Exit Position, *NXP*	−5.38
Mixing chamber diameter, D	4.80

Mixing chamber length, l	41.39
Diffuser length, L	120.15
Diffuser exit diameter, e_d	20

Table 2
Operating conditions simulated in the present work and corresponding to the experiments of Garcia del Valle et al. [1].

Operation	**Primary inlet** (boiler)		**Secondary inlet** (evaporator)		**Outlet** (condenser)		**Ejector performance**	
Point (OP)	$P[kPa]$	$T_{sat}[^oC]$	$P[kPa]$	$T_{sat}[^oC]$	$P[kPa]$	$T_{sat}[^oC]$	$\omega_{exp}[-]$	$P^{ratio}[-]$
1	2598.04	79.37	414.608	10.00	757.222	29.41	0.494	1.826
2	2888.8	84.39	414.608	10.00	826.573	32.48	0.398	1.994
3	3188.14	89.15	414.608	10.00	897.115	35.41	0.339	2.164

Table 3
Thermo-physical properties obtained by the three thermodynamic models for OP2 **(total pressure** $P \in [356.43 - 2950.56]$ kPa **and total temperature** $T \in [16.34 - 95.4]\,^\circ C$ **).**

Properties / Model	**Perfect gas**	**RKS**	**REFPROP 7.0**
kinematic viscosity ($\times 10^{-5}$ $Pa.s$)	1.44	1.44	1.05 – 1.62
Prandtl number (−)	1.54	1.55 – 1.83	0.78 – 1.12
thermal conductivity ($W/m/K$)	0.021	0.021	0.011 – 0.023
heat capacity ($J/kg/K$)	2240.1	2255.5 – 2667.7	871.8 – 1590
density (kg/m^3)	8.64 – 93.03	9.4 – 139.55	11.72 – 144.5

Table 4
Relative deviations ε of the numerical values from the experimental data of Garcia del Valle et al. [1] in terms of the entrainment ratio for OP2 ($\omega_{exp} = 0.398$). Comparisons between the four two-equation models used in their high- (HRN) or low-Reynolds number (LRN) formulation.

Turbulence Model	**Relative deviation** ε **(%)**
standard $k-\varepsilon$ (HRN)	4.27
realizable $k-\varepsilon$ (HRN)	8.79
$k-\varepsilon$ RNG (HRN)	6.03
$k-\omega$ SST (HRN)	6.78
$k-\omega$ SST (LRN)	5.70